

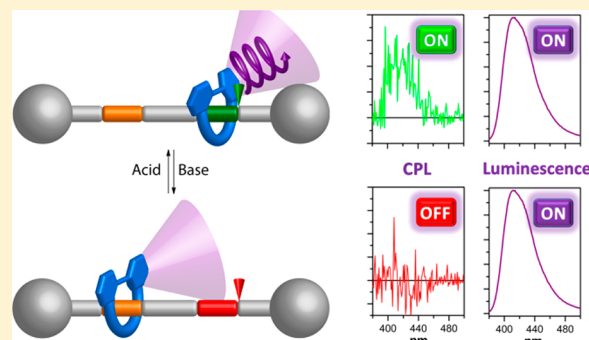
## A [2]Rotaxane-Based Circularly Polarized Luminescence Switch

Arthur H. G. David, Raquel Casares, Juan M. Cuerva,\*<sup>1</sup> Araceli G. Campaña,<sup>1</sup> and Victor Blanco\*<sup>1</sup>

Departamento de Química Orgánica, Facultad de Ciencias, Unidad de Excelencia de Química Aplicada a Biomedicina y Medioambiente (UEQ), Universidad de Granada (UGR), Avda. Fuente Nueva S/N, Granada 18071, Spain

### Supporting Information

**ABSTRACT:** A rotaxane-based molecular shuttle has been synthesized in which the switching of the position of a fluorescent macrocycle on the thread turns “on” or “off” the circularly polarized luminescence (CPL) of the system while maintaining similar fluorescence profiles and quantum yields in both states. The chiroptical activity relies on the chiral information transfer from an ammonium salt incorporating D- or L-phenylalanine residues as chiral stereogenic covalent units to an otherwise achiral crown ether macrocycle bearing a luminescent 2,2'-bipyrene unit when they interact through hydrogen bonding. Each enantiomeric thread induces CPL responses of opposite signs on the macrocycle. Upon addition of base, the switching of the position of the macrocycle to a triazolium group disables the chiral information transfer to the macrocycle, switching “off” the CPL response. The in situ switching upon several acid/base cycles is also demonstrated.



## INTRODUCTION

Over the last three decades, the synthesis and application of mechanically interlocked molecules (MIMs),<sup>1</sup> like rotaxanes<sup>2</sup> or catenanes,<sup>3</sup> has become one of the fields in chemistry that experienced a greater development impelled by the contributions from an increasing number of research groups. The interest for such structures lies not only in the interlocked topologies they present, but also in their growing application in the development of molecular devices and machines able to accomplish different tasks that have grown in complexity over years.<sup>4</sup>

The key feature that makes possible many of those applications of rotaxanes and catenanes is the access given by their interlocked nature to the stimuli-triggered molecular-level control of the motion and relative position of their different components. Thus, if we turn our attention to rotaxanes, especially molecular shuttles in which the position of the macrocycle between different binding sites on the thread can be switched in response to an external stimulus of different nature, they have found application in fields as diverse as molecular electronics,<sup>5</sup> catalysis,<sup>6</sup> controlled-release,<sup>7</sup> achievement of mechanical work or macroscopic movement,<sup>8</sup> or switchable gels.<sup>9</sup> Within this context, control of luminescence by molecular shuttles has been extensively exploited. Thereby, many examples have been reported in which the emissive properties of rotaxane-based molecular shuttles are influenced or modulated in response to the application of an external stimulus.<sup>10</sup>

Despite the extensive work devoted to the synthesis of MIMs and the development of functional molecular machines based on them, the introduction or the use of chirality in such systems has remained much less explored. Taking into account

the utmost importance of chirality in chemistry and other sciences, it is not surprising that the synthesis, study, and applications of chiral rotaxanes and catenanes has recently started to increasingly attract attention.<sup>11</sup> In this sense, the introduction of chiral stereogenic elements,<sup>12</sup> that is, chiral covalent stereogenic centers, chiral stereogenic axis, mechanical planar chirality,<sup>13</sup> or co-conformational covalent or planar chirality,<sup>14</sup> led to interesting applications based precisely on the presence of chirality, such as asymmetric catalysis,<sup>15</sup> chiral anion recognition,<sup>16</sup> or molecular information ratchets.<sup>14a,b</sup>

Unlike the interest in the switching of optical properties like luminescence, the study of chiroptical properties has remained rather unnoticed. It is worth highlighting that, in addition to electronic circular dichroism (ECD), other relevant chiroptical properties, such as vibrational circular dichroism (VCD), optical Raman (ROA), and, more especially, circularly polarized luminescence (CPL),<sup>17</sup> are of interest for different applications. CPL appears as a result of the preferential emission of right or left circularly polarized radiation from the chiral excited state of a molecular system.<sup>18,19</sup> Within this context, CPL emission by well-defined organic or organometallic compounds<sup>20</sup> has been extensively described in recent years. Remarkably, emitted light in these systems has a new degree of freedom at a fixed wavelength, which is of interest in the development of new photonic materials and smart sensing technologies.<sup>21</sup> In particular, the control of this degree of freedom in a dynamic way can be of relevance to encode information in light. That is, dynamic and reversible creation and/or switching of CPL in an emitted radiation can be

Received: July 5, 2019

Published: October 22, 2019

correlated with a writing-and-erasing process. Although some CPL switches<sup>22</sup> have been described, new approaches to CPL-switching are required to fully implement this appealing property in complex devices.

MIMs have been successfully implemented in the switching of a variety of properties even in such complex devices. However, although chiral MIMs and the corresponding ECD studies have been described, chiroptical switching processes have been scarcely studied. The examples described, mainly reported by Leigh and co-workers, are restricted to the modulation or switching of ECD (Figure 1a).<sup>23</sup> If we move to

Therefore, it is clear that much more fundamental research is still required to fully implement and understand the modulation of chiroptical properties, especially CPL, in interlocked molecules. In this context, here we report the first example of the “on”–“off” switching of CPL in a rotaxane-based molecular shuttle controlled by the application of an external stimulus (Figure 1c). Remarkably, the total emission, that is, luminescence of the fluorophore, is maintained in both “on” and “off” CPL states.

## RESULTS AND DISCUSSION

**Concept and System Design.** The design of the system and its prospective operation are shown in Figure 2. It consists of a [2]rotaxane formed by a crown ether macrocycle incorporating an emissive 2,2'-bipyrene unit and a thread bearing a secondary amine/ammonium unit derived from L/D-phenylalanine and a triazolium ring as the binding sites for the macrocycle, similar to that developed by Leigh and co-workers for a switchable catalyst.<sup>15b</sup>

The proposed operation is based on two main features. On one hand, the presence of a CPL response relies on the chiral information transfer from the chiral secondary amine on the thread to the otherwise easy-to-racemize macrocycle, which incorporates the luminescent 2,2'-bipyrene as fluorophore. This transfer of the chiral information between the mechanically bound components of an interlocked structure has been demonstrated to induce a chiral environment on achiral motifs and has been exploited in applications such as asymmetric catalysis,<sup>15a,e</sup> the induction or switching of ECD,<sup>23,26</sup> or the control of the helical structure of polymers.<sup>27</sup> In this case, this chirality transfer would induce a preferential spatial arrangement of the two rings of the 2,2'-bipyrene moiety when the crown ether macrocycle is located around the ammonium unit as a result of the chiral environment created by the phenylalanine residue.<sup>28</sup> Therefore, one of the possible chiral conformations of the macrocycle should be preferentially formed due to that the energetic degeneration between both *R* and *S* enantiomeric conformations is now broken. Moreover, it is also expected the conformational flexibility of the 2,2'-bipyrene subunit in such supramolecular arrangement to be hampered, yielding a neat chiral configuration. If such chiral configuration is preserved in the excited state, a CPL response should be observed.

On the other hand, to enable the possibility of turning “on” or “off” the induced-CPL emission of the 2,2'-bipyrene moiety, we chose the well-known acid/base-promoted switching mechanism of crown ether macrocycles between secondary amine/ammonium and triazolium salts binding sites, first developed by Coutrot and co-workers.<sup>6b,10d,13c,29,30</sup> Protonation or deprotonation of the secondary amine should promote the shuttling of the position of the macrocycle between the binding sites on the thread, as previously demonstrated by Leigh and co-workers in a similar thread.<sup>15b</sup> Thus, when the thread is protonated, the ammonium unit is the preferred binding site for the macrocycle, and this remains located around it. As a result, the chirality transfer between thread and macrocycle would be enabled, activating the CPL emission from the 2,2'-bipyrene unit. On the contrary, upon deprotonation of the ammonium salt to form the neutral secondary amine, the triazolium ring binds more strongly to the macrocycle, which shuttles toward this second station. As the distance between the macrocyclic component and the chiral center on the thread increases, the 2,2'-bipyrene unit

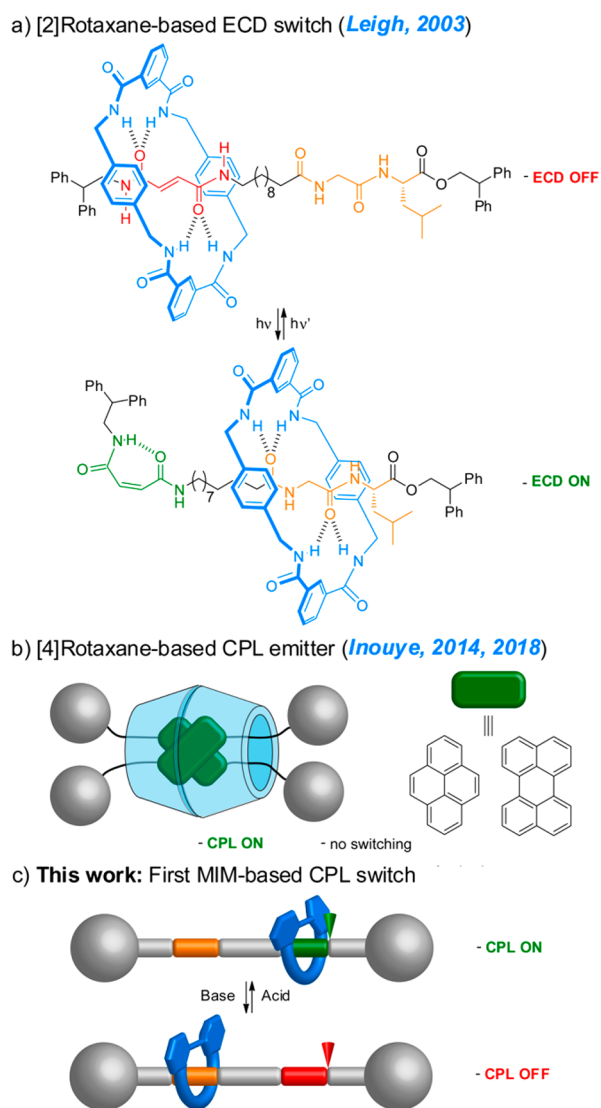


**Figure 1.** (a and b) Related previous work and (c) contribution of this study.

CPL, it becomes clear that the study of this property in MIMs is yet at a very early stage, being limited to one kind of system. Thus, Inouye and co-workers reported two cyclodextrin-based [4]rotaxanes that exhibited CPL emission. This response arises from the excimers formed by two pyrene or perylene moieties from two different threads within the cavity arranged by two cyclodextrin units acting as macrocycles (Figure 1b).<sup>24</sup> Beyond that and to the best of our knowledge, the switching of CPL in rotaxanes or catenanes has not yet been reported.

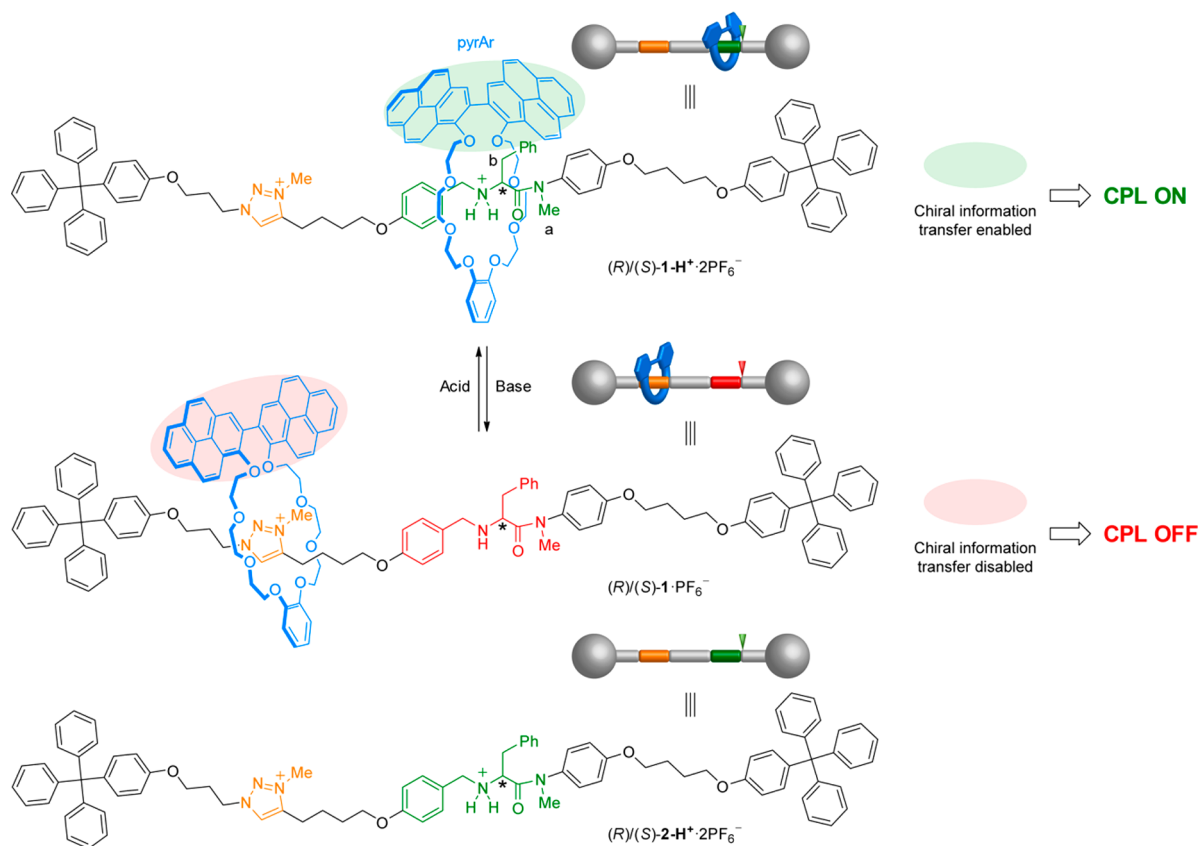


**Figure 2.** “On”–“off” switching of the CPL emission of rotaxanes  $(R)/(S)\text{-}1\text{-H}^+\cdot 2\text{PF}_6^-$  based on the activation/deactivation of chiral information transfer from the thread to the luminescent macrocycle controlled by the acid/base-promoted shuttling of the macrocycle position on the thread.

would be less influenced by the amino acid residue, no longer able to generate a chirally perturbing environment<sup>31</sup> or chirotopic space on the fluorophore. As a result, an equal population of conformational enantiomers of the 2,2'-bipyrene unit could be formed again due to the absence of a chiral environment, thus losing its CPL emission signal without altering the fluorescence of the system. The latter is just originated by the 2,2'-bipyrene unit of macrocycle **8** and should be independent of the inclusion of the fluorophore within a chiral environment. Interestingly, the exclusive switch of CPL while keeping a similar fluorescence emission is especially challenging, and very few examples achieving such control have been reported to date.<sup>22e,f</sup>

As shown, the 2,2'-bipyrene plays a key role as this moiety fulfills the two main requirements needed to ensure the success of the design. On one hand, this group is luminescent as required to have any CPL signal. On the other hand, the link of the two pyrene units through the C-2 position allows the interconversion between the conformers in the absence of any chiral space and the induction of a preferred atropisomer when located in a chiral environment, the requirement to have an “on”–“off” CPL switch.

**Synthesis and Characterization.** To prepare the target rotaxanes, we initially synthesized the 2,2'-bipyrene crown ether **8** (Figure 3a), starting from 2-bromo-1-hydroxypyrene (**3**),<sup>32</sup> which was first protected as the corresponding methyl ether to obtain pyrene derivative **4**. We then tackle the key step in the synthetic route toward the macrocycle, which was the formation of the 2,2'-bipyrene derivative **5**. This was achieved by applying a palladium-catalyzed cross-coupling of aryllithium

derivatives and aryl bromides developed by Feringa and co-workers that allows the dimerization of aryl bromides, even substituted in the *ortho* position, in the presence of <sup>t</sup>BuLi in good yields.<sup>33</sup> Following this methodology, we obtained 2,2'-bipyrene-1,1'-diol (**5**) after deprotection of the methyl ether groups with  $\text{BF}_3\cdot\text{SMe}_2$ . Finally, reaction of **5** with the catechol-derived dibromide **7** using <sup>t</sup>BuOK as base and a potassium salt as template afforded the target macrocycle **8** in 34% yield.

The 2,2'-bipyrene-containing crown ether **8** was characterized by NMR and MS techniques (see the Supporting Information). In addition, single crystals of its potassium complex  $8\text{K}^+$  were obtained and studied by X-ray diffraction. Although of moderate quality, the solid-state structure confirmed the structure of the macrocycle (Figure 3b). It showed the 2,2'-bipyrene unit with both pyrenes twisted with a torsion angle of  $59.7^\circ$ . As expected, in the absence of a chiral environment, the two possible conformational enantiomers are present within the structure. The formation of the complex with a  $\text{K}^+$  ion favors the crown ether to adopt a twisted conformation around the cation that allows the coordination of the O atoms to the  $\text{K}^+$  cation with  $\text{K}\text{-O}$  distances within 2.45–2.61 Å.

For the synthesis of rotaxanes  $(R)/(S)\text{-}1\text{-H}^+\cdot 2\text{PF}_6^-$ , we followed the threading-and-capping approach (Scheme 1),<sup>25</sup> starting from monostoppered alkyne derivatives  $(R)/(S)\text{-}11\text{-H}^+\cdot \text{PF}_6^-$ , which incorporate a chiral secondary ammonium salt as template for the crown ether macrocycle, prepared by reductive amination between aldehyde **10** and the primary amine obtained by Boc-removal from  $(R)/(S)\text{-}9$  followed by protonation and counterion exchange. For the mechanical

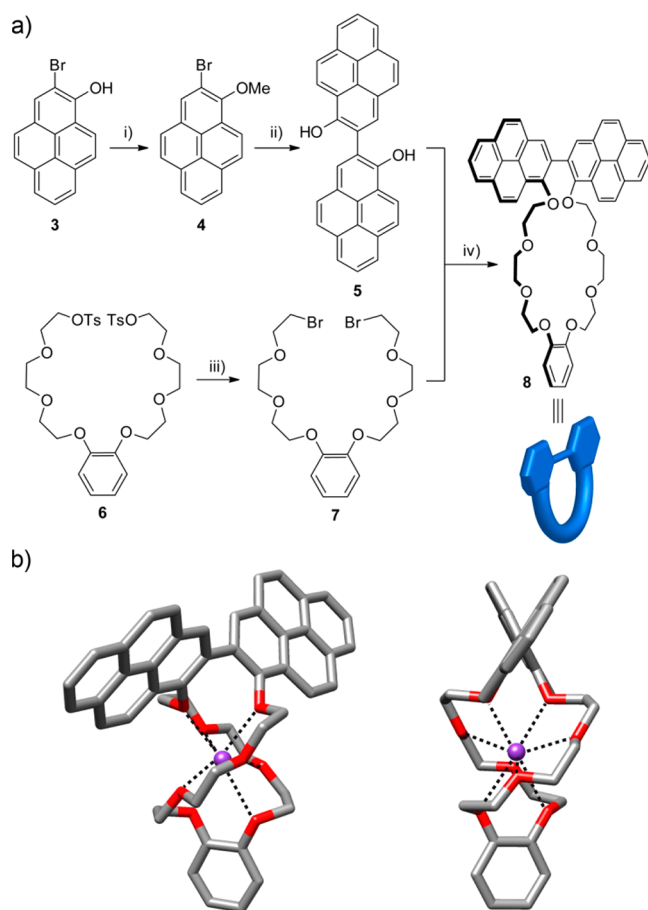


**Figure 3.** (a) Synthesis of benzo-1,1'-bipyreno-26-crown-8 macrocycle (**8**). Reagents and conditions: (i) MeI,  $K_2CO_3$ , acetone, 0 °C to reflux, 18 h, 83%; (ii) (1)  $tBuLi$ , Pd(dba) $_2$ , XPhos, toluene, rt, 20 h, 79%; (2)  $BF_3 \cdot SMe_2$ ,  $CH_2Cl_2$ , rt, 6 h, 26%; (iii) LiBr, acetone, reflux, O/N, 92%; (iv)  $tBuOK$ ,  $KPF_6$ ,  $^{n}Bu_4NI$ , 0.6 mM, dioxane, rt to reflux, 24 h, 34%. (b) Front (left) and side (right) views of the stick representation of the X-ray diffraction structure of **8CK** $^+$ . The coordination bonds between K and the crown ether O atoms are shown with dashed lines. Hydrogen atoms and the  $PF_6^-$  counterion have been omitted for clarity. Color coding: C, gray; O, red; K, purple.

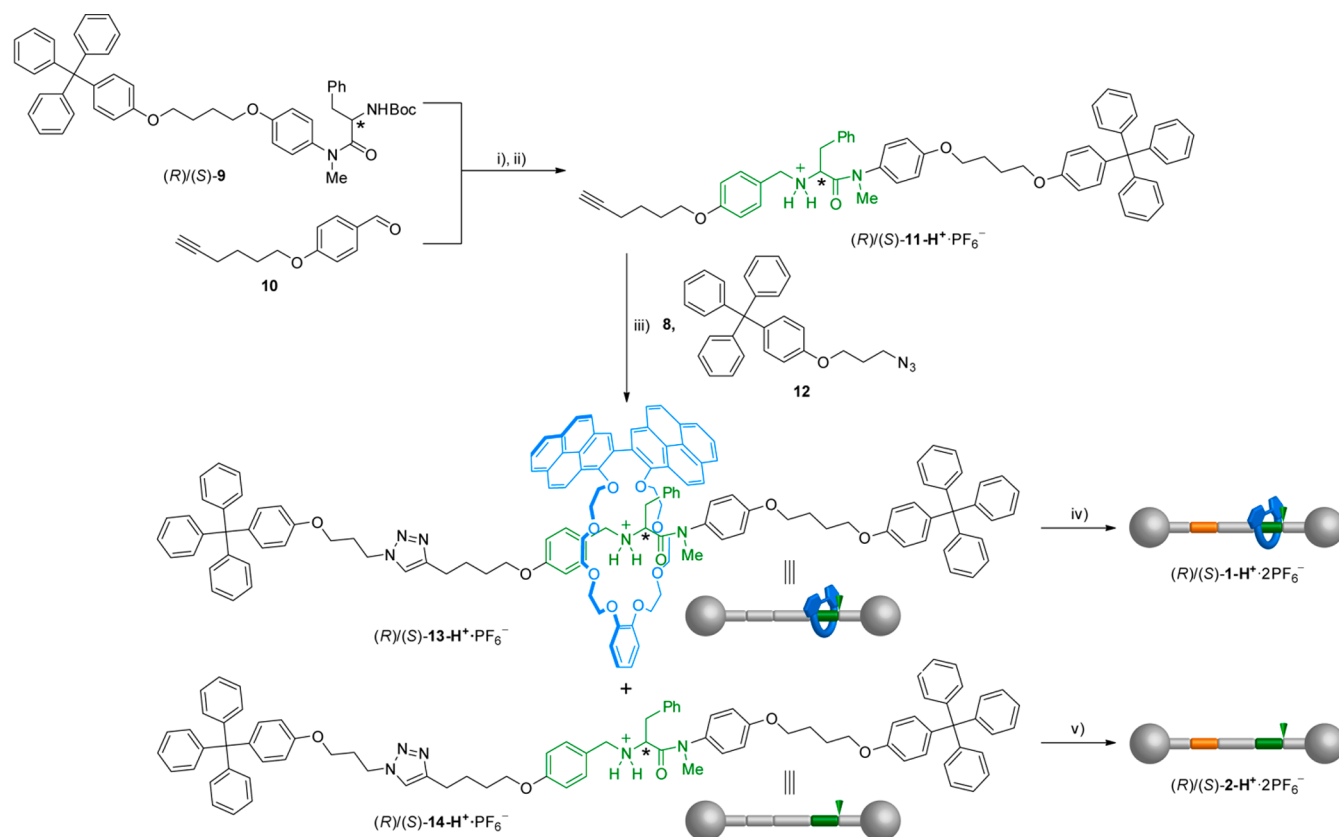
bond-forming step, we used the click CuAAC reaction<sup>34</sup> between azide **12** and alkyne (*R*)/(*S*)-**11-H** $^+$  $\cdot PF_6^-$  in the presence of macrocycle **8**, affording the interlocked system (*R*)/(*S*)-**13-H** $^+$  $\cdot PF_6^-$  in 19–35%. Methylation of the resulting triazole ring with MeI followed by counterion exchange finally yielded target rotaxanes (*R*)/(*S*)-**1-H** $^+$  $\cdot 2PF_6^-$ .

It has been pointed out that one the drawbacks associated with the presence of chirality in MIMs could be an increased complexity of the NMR spectra of the systems obtained.<sup>11b</sup> This is indeed the phenomena we observed. When compared to those of macrocycle **8** and free thread **14-H** $^+$  $\cdot PF_6^-$ , the  $^1H$  NMR spectra of rotaxanes **13-H** $^+$  $\cdot PF_6^-$  show a complex pattern in both the aromatic and the aliphatic regions with a high number of signals, some of them overlapped and broad, which prevented its full analysis and assignment. This situation is not surprising taking into account that, as a result of the macrocycle being located near to the phenylalanine residue, a symmetry loss induced by the chiral environment is at least expected.<sup>35</sup> Therefore, a complex NMR spectrum could suggest by itself the presence of an interlocked species.

However, a careful inspection of the  $^1H$  and 2D NMR spectra of **13-H** $^+$  $\cdot PF_6^-$  and their comparison with those of free thread **14-H** $^+$  $\cdot PF_6^-$  allowed us to locate the signal of the amide *N*-methyl group, which can be used as a diagnostic signal (see Figure 4b,c). Upon formation of the rotaxane, the hydrogen atoms of this methyl group are shifted toward lower frequencies ( $\Delta\delta_{Ha} = -0.90$  ppm, Figure 4b,c) as compared to the protonated free thread as a result of the shielding by the aromatic rings of the macrocycle.<sup>36</sup> DOSY NMR experiments also supported the interlocked nature of the system as the signals corresponding to both the macrocycle and the axle exhibited the same diffusion coefficient, showing that both components diffuse as a whole (see Figure 5a). Moreover, the identity of the rotaxane was further confirmed by electrospray high-resolution mass spectrometry (ESI-TOF HRMS). The mass spectra showed a major peak at  $m/z = 2038.9519$  whose exact mass and isotopic distribution nicely match those corresponding to the  $[M - PF_6^-]^+$  ion (see Figures S59 and S60).

The final rotaxanes (*R*)/(*S*)-**1-H** $^+$  $\cdot 2PF_6^-$  were also characterized on the basis of the same experimental evidence. After methylation of the triazolium ring, most of the signals of the  $^1H$  NMR spectrum broadened, but the diagnostic resonance for the amide *N*-methyl hydrogens could still be clearly observed (see Figure 4d). This signal appears at the same chemical shift ( $\delta_{Ha} = 2.31$  ppm, Figure 4c,d) as in **13-H** $^+$  $\cdot PF_6^-$  and is shifted upfield ( $\Delta\delta_{Ha} = -0.87$  ppm) when compared to thread **2-H** $^+$  $\cdot 2PF_6^-$ , showing that the macrocycle remains on the ammonium station despite the triazole ring being methylated, as expected due to the stronger hydrogen-bond interactions the crown ether can establish with the secondary ammonium motif (Figure 4d,f). As for the non-methylated rotaxane precursor, DOSY NMR experiments were also in line with the presence of the rotaxane with both components forming part of a threaded system (Figure S55). ESI-TOF HRMS further supported the proposed structure with three main peaks in the spectra ( $m/z = 1026.9816$ , 2052.9675, and 2198.9368), which correspond to the  $[M - 2PF_6^-]^{2+}$ ,  $[M - H^+ - 2PF_6^-]^+$ , and  $[M - PF_6^-]^+$  ions. Furthermore, the exact mass and the isotopic pattern for the peak corresponding to the  $[M - H^+ - 2PF_6^-]^+$  species are in good agreement with the theoretical data (Figure 5b and Figures S61 and S62).

**Study and Switching of Chiroptical Properties.** Having synthesized and characterized rotaxanes (*R*)/(*S*)-**1-H** $^+$  $\cdot 2PF_6^-$  along with the corresponding free threads and the 2,2'-bipyrene macrocycle, we evaluated the (chiro)optical properties of the different species. The UV–vis absorption spectrum of macrocycle **8** in  $CHCl_3$  shows a structured absorption band between 320 and 400 nm with a maximum centered at 355 nm ( $\epsilon = 57\,494\ M^{-1}\ cm^{-1}$ ) and a small shoulder at 386 nm ( $\epsilon = 1989\ M^{-1}\ cm^{-1}$ ) as the main features. Because of the presence of the pyrene units, this macrocycle is fluorescent when irradiated with UV light ( $\lambda_{exc} = 355$  nm) with an emission band centered at 404 nm (QY = 0.18) (Figure S75). Compound **8** did not show any ECD or CPL signals, as expected for a biphenyl-type compound with a low racemization barrier (Figures S77 and S78). On the contrary, enantiopure free threads (*R*)/(*S*)-**2-H** $^+$  $\cdot 2PF_6^-$  and (*R*)/(*S*)-**14-H** $^+$  $\cdot PF_6^-$  only exhibit bands in their UV–vis spectra at lower wavelengths (240–325 nm) as compared to macrocycle **8** and do not show any emission as a result of the absence of any fluorophore (Figures S79, S80, S82, and S83). Because of the presence of *L/D*-phenylalanine as chiral stereogenic units in

Scheme 1. Synthesis of Rotaxanes (R)/(S)-1-H<sup>+</sup>·2PF<sub>6</sub><sup>-α</sup>

<sup>α</sup>Reagents and conditions: (i) (1) CF<sub>3</sub>CO<sub>2</sub>H, CH<sub>2</sub>Cl<sub>2</sub>, rt, 4 h; (2) **10**, Et<sub>3</sub>N, MeOH, rt, 24 h; (3) NaBH<sub>4</sub>, THF/MeOH, rt, 18 h, 32% (from (R)-**9**) and 34% (from (S)-**9**); (ii) (1) HCl (1.0 M in Et<sub>2</sub>O), CH<sub>2</sub>Cl<sub>2</sub>, rt, 8 h; (2) KPF<sub>6</sub>, CH<sub>2</sub>Cl<sub>2</sub>/acetone/H<sub>2</sub>O, rt, 16 h, 98% (for (R)-**11-H<sup>+</sup>·PF<sub>6</sub><sup>-</sup>**) and 91% (for (S)-**11-H<sup>+</sup>·PF<sub>6</sub><sup>-</sup>**); (iii) Cu(CH<sub>3</sub>CN)<sub>4</sub>PF<sub>6</sub>, TBTA, CH<sub>2</sub>Cl<sub>2</sub>, rt, 3 d, 35% (for (R)-**13-H<sup>+</sup>·PF<sub>6</sub><sup>-</sup>**) and 19% (for (S)-**13-H<sup>+</sup>·PF<sub>6</sub><sup>-</sup>**); (iv) (1) CH<sub>3</sub>I, rt, 4 d; (2) KPF<sub>6</sub>, CH<sub>2</sub>Cl<sub>2</sub>/acetone/H<sub>2</sub>O, rt, 5 h, 68% (for (R)-**1-H<sup>+</sup>·2PF<sub>6</sub><sup>-</sup>**) and 55% (for (S)-**1-H<sup>+</sup>·2PF<sub>6</sub><sup>-</sup>**); (v) (1) CH<sub>3</sub>I, rt, 4 d; (2) KPF<sub>6</sub>, CH<sub>2</sub>Cl<sub>2</sub>/acetone/H<sub>2</sub>O, rt, 18 h, 58% (for (R)-**2-H<sup>+</sup>·2PF<sub>6</sub><sup>-</sup>**) and 98% (for (S)-**2-H<sup>+</sup>·2PF<sub>6</sub><sup>-</sup>**).

their structure, the threads show ECD signals below 300 nm, but its nonemissive behavior precludes the potential presence of any CPL response (Figures S81 and S84).

On the other hand, rotaxanes (R)/(S)-**13-H<sup>+</sup>·PF<sub>6</sub><sup>-</sup>** and (R)/(S)-**1-H<sup>+</sup>·2PF<sub>6</sub><sup>-</sup>** display a UV-vis spectra with two main bands, one centered at 273 nm, while the second one is located in the 320–400 nm region with a maximum centered at 355 nm ( $\epsilon = 55\,230\text{ M}^{-1}\text{ cm}^{-1}$ ) and shows a vibronic structure, with a shape and energy similar to those of the main absorption band of macrocycle **8** (Figure 6a, middle, and Figures S85 and S93). As expected, upon excitation with UV light ( $\lambda_{\text{exc}} = 355\text{ nm}$ ), all rotaxanes show a fluorescent emission band ( $\lambda_{\text{em}} = 404\text{ nm}$ , QY = 0.19 for **13-H<sup>+</sup>·PF<sub>6</sub><sup>-</sup>** and QY = 0.11 for **1-H<sup>+</sup>·2PF<sub>6</sub><sup>-</sup>**), again with a shape similar to and the same wavelength range (380–500 nm) as that of **8**, in accordance with the 2,2'-bipyrene unit being the fluorophore responsible for the luminescence properties (Figure 6a, middle, and Figure S85). Nevertheless, as a result of the incorporation of both the luminescent achiral macrocycle and any of the nonemissive homochiral threads into a rotaxane architecture, a clear change in the chiroptical properties is observed. Thus, all rotaxanes show similar ECD spectra with several bands within 300–425 nm, where the absorption can be attributed mainly to the pyrene units (Figure 6a, top, and Figures S88–S90, S95, and S96). The phenylalanine having D- or L-configuration results in the ECD spectra of the corresponding rotaxanes being mirror images. Accordingly, (S)-**1-H<sup>+</sup>·2PF<sub>6</sub><sup>-</sup>** showed a negative

Cotton effect at 355 nm ( $|\Delta\epsilon| \approx 4\text{ M}^{-1}\text{ cm}^{-1}$ ,  $g_{\text{abs}} = \Delta\epsilon/\epsilon \approx 7 \times 10^{-5}$ ) and a positive one at the lowest energy transition at 400 nm ( $|\Delta\epsilon| \approx 0.5\text{ M}^{-1}\text{ cm}^{-1}$ ,  $g_{\text{abs}} = \Delta\epsilon/\epsilon \approx 3 \times 10^{-4}$ ).

Moreover, upon excitation with UV light ( $\lambda_{\text{exc}} = 355\text{ nm}$ ), CPL responses covering the range of the emission band are observed for the rotaxanes. CPL is usually evaluated with the luminescence dissymmetry ratio ( $g_{\text{lum}}$ ), calculated as  $g_{\text{lum}} = 2(I_L - I_R)/(I_L + I_R)$ , with  $I_L$  and  $I_R$  being the intensities of left and right circularly polarized emitted light. Both (R)/(S)-**13-H<sup>+</sup>·PF<sub>6</sub><sup>-</sup>** and (R)/(S)-**1-H<sup>+</sup>·2PF<sub>6</sub><sup>-</sup>** rotaxanes afforded  $|g_{\text{lum}}|$  values of  $\sim 0.5 \times 10^{-3}$ . These values are in agreement with previously reported chiral binaphthyl-based systems.<sup>37</sup> It is worth noting that for homogeneous systems, the dissymmetry ratio  $g_{\text{lum}}$  can be expressed theoretically in terms of the electric and magnetic dipole transition moments  $\mu$  and  $m$ ,  $g_{\text{lum}} = 4(|\mu| \cdot |m| \cdot \cos \theta)/(|\mu|^2 + |m|^2) \approx 4R/D$ , where  $R$  and  $D$  are the rotational and dipole strengths, respectively, for the S<sub>1</sub>-to-S<sub>0</sub> transition.<sup>18</sup> Consequently, weak magnetic transitions, as expected for simple biphenyl-type emitters, joined to reasonably luminescent compounds yield weak, although observable, CPL spectra in the range of  $10^{-4}$ .

The enantiomeric forms gave CPL signals of opposite  $g_{\text{lum}}$  signs, as expected for a pure CPL response (Figure 6a, bottom, and Figures S91, S92, and S97).<sup>18</sup> Both the  $g_{\text{lum}}$  values and the signs are in good agreement with the corresponding values and signs of the  $g_{\text{abs}}$  of the lowest energy band in the corresponding ECD spectrum (inset of Figure 6a, top, and Figure S96), being

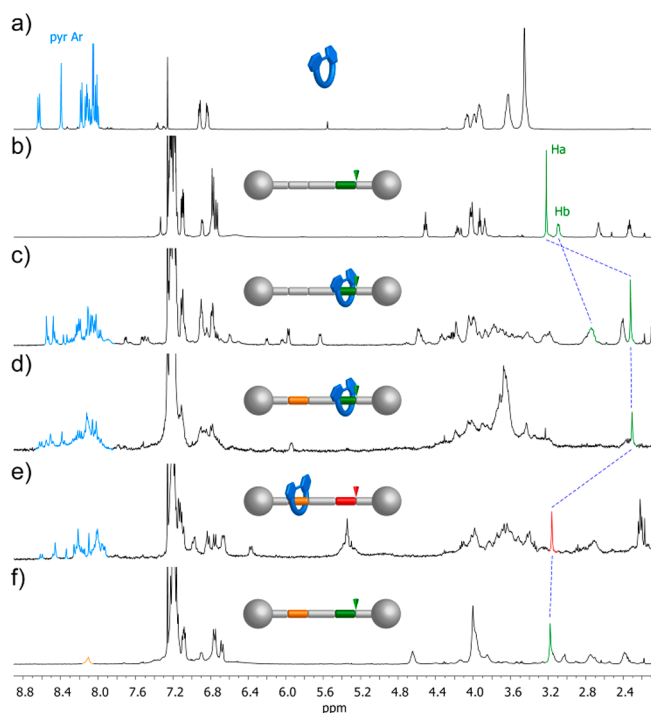


**Figure 4.** Partial  $^1\text{H}$  NMR spectra ( $\text{CDCl}_3$ ) of (a) macrocycle **8** (500 MHz); (b) thread **14**- $\text{H}^+\cdot\text{PF}_6^-$  (500 MHz); (c) rotaxane **13**- $\text{H}^+\cdot\text{PF}_6^-$  (500 MHz); (d) rotaxane **1**- $\text{H}^+\cdot 2\text{PF}_6^-$  (400 MHz); (e) rotaxane **1**- $\text{PF}_6^-$  (400 MHz); and (f) thread **2**- $\text{H}^+\cdot 2\text{PF}_6^-$  (400 MHz). Lettering and color coding are defined in Figure 2.

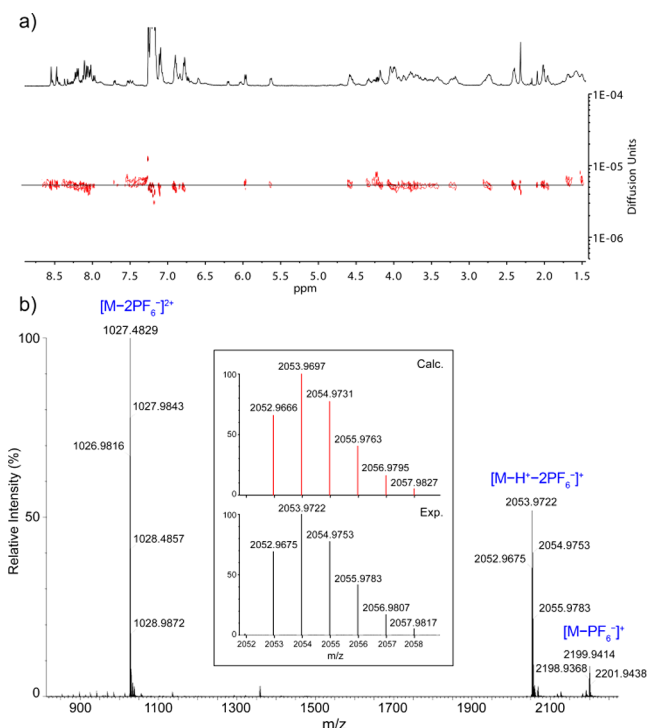


**Figure 5.** (a) DOSY NMR spectra (500 MHz,  $\text{CDCl}_3$ ) of rotaxane **13**- $\text{H}^+\cdot\text{PF}_6^-$ ; and (b) HRMS (ESI $^+$ -TOF) spectrum of rotaxane **1**- $\text{H}^+\cdot 2\text{PF}_6^-$ . Inset: Experimental (bottom) and calculated (top) isotopic distributions for the peak corresponding to the ion  $[\text{M} - \text{H}^+ - 2\text{PF}_6^-]^+$ .

positive for the (*S*) enantiomers of both rotaxanes and negative for the ones with (*R*) configuration on the amino acid.<sup>38</sup> The

results obtained for the chiroptical properties are by themselves proof of the interlocked nature of the structures studied, taking into account that neither the ECD nor the CPL spectra of a mixture of thread (*S*)-**2**- $\text{H}^+\cdot\text{PF}_6^-$  and macrocycle **8** (ca.  $1 \times 10^{-5}$  M of each component) show any of the features observed in those recorded for the corresponding rotaxane (see Figures S106 and S107). Therefore, they can be only explained by the chiral information transfer between the phenylalanine unit on the thread and the 2,2'-bipyrene unit. The different sign of the bands on the ECD and CPL spectra upon change of the configuration of the amino acid residue, resulting in mirror image spectra, clearly supports this chiral induction as each of the phenylalanine configurations would induce a different preferential atropisomer-based configuration on the 2,2'-bipyrene moiety. Another control experiment that highlights the importance of the interlocked structures was the study of the chiroptical properties of an equimolar mixture of (*S*)-**11**- $\text{H}^+\cdot\text{PF}_6^-$  and macrocycle **8** (ca.  $1 \times 10^{-5}$  M of each component). Again, the CPL spectra did not show any signal, revealing the need of an interlocked rotaxane to observe chiroptical responses in this system (Figures S109 and S110). This result can be attributed to the component not forming a proportion of the supramolecular complex high enough at the concentration used for its chiroptical properties being observed.

After demonstrating the CPL emission of the system, we decided to evaluate its possible “on”–“off” switching taking advantage of the incorporated well-known shuttling mechanism. In fact, addition of  $\text{K}_2\text{CO}_3$  to rotaxanes (*R*)/(*S*)-**1**- $\text{H}^+\cdot 2\text{PF}_6^-$  with the aim of deprotonating the secondary amine unit and forming (*R*)/(*S*)-**1**- $\text{PF}_6^-$  dramatically influenced their chiroptical properties. Neither the UV–vis nor the fluorescence spectra experienced important changes. For the latter, both the shape of the emission band ( $\lambda_{\text{max}} = 401$  nm) and the corresponding quantum yield ( $\text{QY} = 0.11$ ) remained essentially unaltered (Figure 6b, middle). However, in both the ECD and the CPL spectra, no signals corresponding to the 2,2'-bipyrene moiety could be detected, and the bands that appeared prior to the addition of the base were no longer present (Figure 6b, top and bottom, and Figure S100).

$^1\text{H}$  NMR spectroscopy allowed us to gain insight into the effect of the base addition on the rotaxane. The amide *N*-methyl signal shifted downfield in comparison to **1**- $\text{H}^+\cdot 2\text{PF}_6^-$  ( $\Delta\delta_{\text{Ha}} = 0.85$  ppm) with a chemical shift ( $\delta_{\text{Ha}} = 3.16$  ppm) similar to that in free thread **2**- $\text{H}^+\cdot 2\text{PF}_6^-$  (Figure 4d–f). Therefore, the NMR experiment endorses the switching of the position of the macrocycle from the secondary amine to the triazolium ring as a result of the deprotonation of the former by addition of base.

Addition of  $\text{CF}_3\text{CO}_2\text{H}$  to (*R*)/(*S*)-**1**- $\text{PF}_6^-$  restored the chiroptical properties as both the ECD and the CPL spectra are similar to those initially measured for (*R*)/(*S*)-**1**- $\text{H}^+\cdot 2\text{PF}_6^-$ , again with no evident changes in the absorption or emission spectra (Figures 6c and S101).<sup>39</sup> Therefore, the key feature of the system is that the CPL response can be switched “on” or “off” by addition of acid or base without altering the luminescence profile, yielding the first rotaxane-based CPL switch.<sup>40</sup>

Finally, taking advantage of the interlocked architecture, we attempted the in situ switching of the CPL response. Starting from (*S*)-**1**- $\text{H}^+\cdot 2\text{PF}_6^-$ , with a  $g_{\text{lum}}$  value of  $\sim 0.5 \times 10^{-3}$ , the CPL spectra were recorded after consecutive cycles of  $\text{K}_2\text{CO}_3$  and  $\text{CF}_3\text{CO}_2\text{H}$  addition to control the position of the

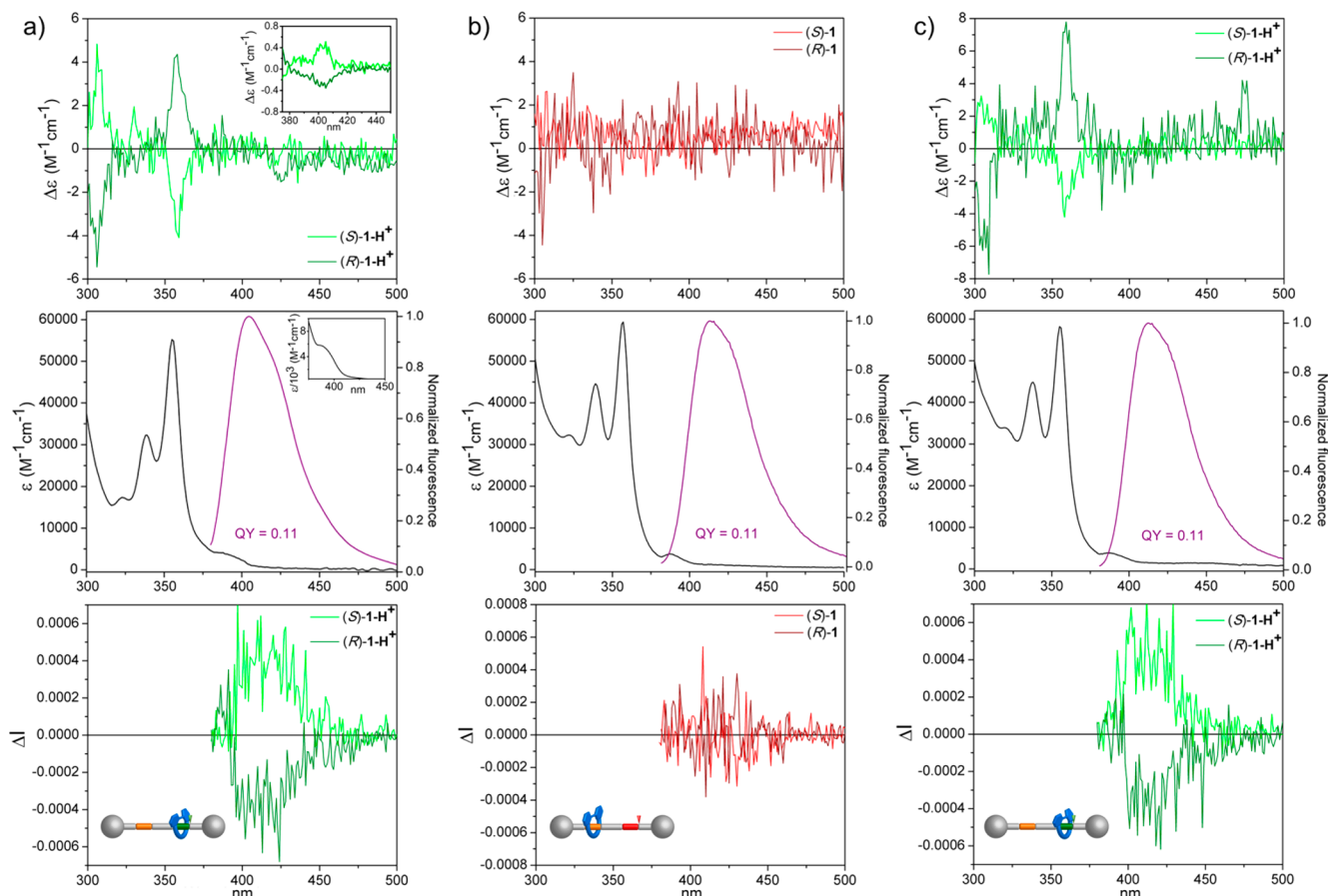


**Figure 6.** ECD (ca.  $1 \times 10^{-5}$  M) (top), UV-vis absorption (ca.  $1 \times 10^{-5}$  M) (black line) and fluorescence ( $\lambda_{exc} = 355$  nm) (ca.  $1 \times 10^{-5}$  M) (purple line) (middle), and CPL in normalized  $\Delta I$  scale ( $\lambda_{exc} = 355$  nm) (ca.  $1 \times 10^{-5}$  M) (bottom) spectra ( $CHCl_3$ ) of (a)  $1-H^+ \cdot 2PF_6^-$ ; (b)  $1-PF_6^-$ ; and (c)  $1-H^+$ , obtained by protonation of  $1-PF_6^-$  with a solution of  $CF_3CO_2H$  in  $CHCl_3$ . Inset (a): Partial ECD (ca.  $1 \times 10^{-4}$  M) spectrum showing the lowest energy band (top) and partial UV-vis spectrum (ca.  $1 \times 10^{-4}$  M) showing the longest wavelength absorption (bottom).

macrocycle on the thread. The data show that, for three complete cycles, the addition of base disables the CPL response with  $g_{lum}$  values close to 0, while the reprotonation restores the CPL signal (Figure 7), and, in any case, fluorescence emission remains essentially unaltered throughout (around 10% variation).

After each cycle, some decrease in the restored CPL signal is observed, probably due to some degradation observed in the deprotonated “off” state. We assume that an oxidation to amine *N*-oxide is taking place precluding the full restoration of the CPL signal upon treatment with  $CF_3CO_2H$ . This

degradation was minimized, although unfortunately not completely suppressed, by carrying out the experiments under Ar atmosphere.<sup>41</sup> In any case, the statistical tests performed on the CPL signals of the “on” and “off” states of each cycle show that, despite this degradation, the responses for the “on” states are significantly higher than those of the “off” states and can be clearly distinguished (see Supporting Information for further details). Therefore, the CPL “on”–“off” switching character of the presented MIM is fully demonstrated.

## CONCLUSIONS

Chiroptical responses, especially CPL, are attracting increasing attention as relevant properties in the design of advanced photonic materials or in optoelectronic or sensing applications. In this sense, not only systems that exhibit CPL signals are relevant, but also those in which this chiroptical response can be modulated in a controlled fashion upon application of external stimuli. Within this context, chiral enantiopure rotaxane-based molecular shuttles with well-known switching mechanisms represent a platform with an excellent potential to be exploited in the development of such materials. This strategy is linked to the increasing attention the chirality in MIMs is receiving recently and represents an example of the properties available ahead of the development of chiral rotaxanes and catenanes.

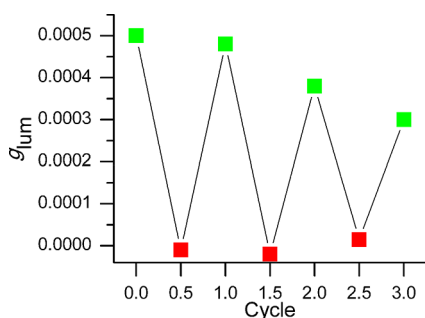


**Figure 7.** In situ “off”–“on” switching of the CPL emission of (S)- $1-H^+ \cdot 2PF_6^-$  after consecutive addition of base ( $K_2CO_3$ , red ■) and acid ( $CF_3CO_2H$ , green ■).

Thus, in this work, we present the first CPL “on”–“off” switch based on a MIM, in this case, a [2]rotaxane molecular shuttle. The chiroptical properties of this design rely on the chiral information transfer that occurs when a crown-ether macrocycle bearing a luminescent 2,2'-bipyrene unit interacts through hydrogen bonding with a secondary ammonium unit on the thread incorporating D- or L-phenylalanine motifs. As a result, one 2,2'-bipyrene atropisomer is preferentially formed and a CPL signal is observed, with different sign depending on the configuration of the chiral covalent stereogenic unit. Enabling or disabling the chiral information transfer by switching the position of the macrocycle on the thread by addition of acid or base allows the “on”–“off” switching of the CPL emission. Remarkably, the fluorescence profile or its corresponding quantum yield did not become altered. Finally, we demonstrate that the CPL response can be switched in situ by subsequent addition of base and acid for several complete cycles.

These proof-of-concept results not only reinforce the potential of molecular machines, expanding the already wide range of applications in which they have proved useful, but also open a new strategy that can be explored to develop systems of increasing efficiency and robustness that allow the selective control and switching of CPL and perhaps other chiroptical properties, which are called to play an important role in a new generation of materials.

## ■ ASSOCIATED CONTENT

### Supporting Information

The Supporting Information is available free of charge on the ACS Publications website at DOI: 10.1021/jacs.9b07143.

Experimental procedures, synthetic and characterization details, NMR spectra, ESI–MS spectra, crystallographic data, HPLC traces for final compounds, statistical tests on the CPL signals, and additional figures (PDF)

X-ray crystallographic data (CIF)

## ■ AUTHOR INFORMATION

### Corresponding Authors

\*jmcuerva@ugr.es

\*victorblancos@ugr.es

### ORCID

Juan M. Cuerva: 0000-0001-6896-9617

Araceli G. Campaña: 0000-0001-5483-5642

Victor Blanco: 0000-0002-6809-079X

### Notes

The authors declare no competing financial interest.

## ■ ACKNOWLEDGMENTS

We acknowledge the Ministerio de Economía y Competitividad (MINECO FEDER, Spain; CTQ2017-85454-C2-1-P, UNGR15-CE-3478), the Ministerio de Ciencia, Innovación y Universidades (MICIU, Spain; PGC2018-101181-B-I00 AEI/FEDER, UE), and the European Research Council (ERC) under the European Union's Horizon 2020 research and innovation program (ERC-2015-STG-677023) for financial support. A.G.C. acknowledges MINECO for a “Ramón y Cajal” contract (RyC-2013-12943). We also thank Universidad de Granada (UGR) (Visiting Scholars PP2016-VS01 and “Intensificación de la Investigación” PP2017-PRI-I-02 programmes from the “Plan Propio de Investigación”) for further

financial support. We thank Prof. L. Cuadros-Rodríguez and Dr. Ana M. Jiménez-Carvelo for their assistance with the statistical tests.

## ■ REFERENCES

- (1) (a) Sauvage, J. P.; Dietrich-Buchecker, C. *Molecular Catenanes, Rotaxanes and Knots: A Journey Through the World of Molecular Topology*; Wiley-VCH: Weinheim, 1999. (b) Bruns, C. J.; Stoddart, J. F. *The Fundamentals of Making Mechanical Bonds*; John Wiley & Sons: Hoboken, 2016.
- (2) Xue, M.; Yang, Y.; Chi, X.; Yan, X.; Huang, F. Development of Pseudorotaxanes and Rotaxanes: From Synthesis to Stimuli-Responsive Motions to Applications. *Chem. Rev.* **2015**, *115*, 7398–7501.
- (3) (a) Evans, N. H.; Beer, P. D. Progress in the synthesis and exploitation of catenanes since the Millennium. *Chem. Soc. Rev.* **2014**, *43*, 4658–4683. (b) Gil-Ramírez, G.; Leigh, D. A.; Stephens, A. J. Catenanes: Fifty Years of Molecular Links. *Angew. Chem., Int. Ed.* **2015**, *54*, 6110–6150.
- (4) (a) Balzani, V.; Credi, A.; Raymo, F. M.; Stoddart, J. F. Artificial Molecular Machines. *Angew. Chem., Int. Ed.* **2000**, *39*, 3348–3391. (b) Kay, E. R.; Leigh, D. A.; Zerbetto, F. Synthetic Molecular Motors and Mechanical Machines. *Angew. Chem., Int. Ed.* **2007**, *46*, 72–191. (c) van Dongen, S. F. M.; Cantekin, S.; Elemans, J. A. A. W.; Rowan, A. E.; Nolte, R. J. M. Functional interlocked systems. *Chem. Soc. Rev.* **2014**, *43*, 99–122. (d) Erbas-Cakmak, S.; Leigh, D. A.; McTernan, C. T.; Nussbaumer, A. L. Artificial Molecular Machines. *Chem. Rev.* **2015**, *115*, 10081–10206. (e) Kassem, S.; van Leeuwen, T.; Lubbe, A. S.; Wilson, M. R.; Feringa, B. L.; Leigh, D. A. Artificial molecular motors. *Chem. Soc. Rev.* **2017**, *46*, 2592–2621.
- (5) (a) Collier, C. P.; Wong, E. W.; Belohradský, M.; Raymo, F. M.; Stoddart, J. F.; Kuekes, P. J.; Williams, R. S.; Heath, J. R. Electronically Configurable Molecular-Based Logic Gates. *Science* **1999**, *285*, 391–394. (b) Green, J. E.; Wook Choi, J.; Boukai, A.; Bunimovich, Y.; Johnston-Halperin, E.; DeIonno, E.; Luo, Y.; Sheriff, B. A.; Xu, K.; Shik Shin, Y.; Tseng, H.-R.; Stoddart, J. F.; Heath, J. R. A 160-kilobit molecular electronic memory patterned at 1011 bits per square centimetre. *Nature* **2007**, *445*, 414.
- (6) (a) Berná, J.; Alajarin, M.; Orenes, R.-A. Azodicarboxamides as Template Binding Motifs for the Building of Hydrogen-Bonded Molecular Shuttles. *J. Am. Chem. Soc.* **2010**, *132*, 10741–10747. (b) Blanco, V.; Carlone, A.; Hänni, K. D.; Leigh, D. A.; Lewandowski, B. A Rotaxane-Based Switchable Organocatalyst. *Angew. Chem., Int. Ed.* **2012**, *51*, 5166–5169. (c) Blanco, V.; Leigh, D. A.; Lewandowska, U.; Lewandowski, B.; Marcos, V. Exploring the Activation Modes of a Rotaxane-Based Switchable Organocatalyst. *J. Am. Chem. Soc.* **2014**, *136*, 15775–15780. (d) Kwan, C.-S.; Chan, A. S. C.; Leung, K. C.-F. A Fluorescent and Switchable Rotaxane Dual Organocatalyst. *Org. Lett.* **2016**, *18*, 976–979. (e) Eichstaedt, K.; Jaramillo-García, J.; Leigh, D. A.; Marcos, V.; Pisano, S.; Singleton, T. A. Switching between Anion-Binding Catalysis and Aminocatalysis with a Rotaxane Dual-Function Catalyst. *J. Am. Chem. Soc.* **2017**, *139*, 9376–9381.
- (7) (a) Nguyen, T. D.; Liu, Y.; Saha, S.; Leung, K. C. F.; Stoddart, J. F.; Zink, J. I. Design and Optimization of Molecular Nanovalves Based on Redox-Switchable Bistable Rotaxanes. *J. Am. Chem. Soc.* **2007**, *129*, 626–634. (b) Fernandes, A.; Viterisi, A.; Coutrot, F.; Potok, S.; Leigh, D. A.; Aucagne, V.; Papat, S. Rotaxane-Based Propeptides: Protection and Enzymatic Release of a Bioactive Pentapeptide. *Angew. Chem., Int. Ed.* **2009**, *48*, 6443–6447. (c) Martínez-Cuevas, A.; Valero-Moya, S.; Alajarin, M.; Berna, J. Light-responsive peptide [2]rotaxanes as gatekeepers of mechanised nanocontainers. *Chem. Commun.* **2015**, *51*, 14501–14504.
- (8) (a) Berná, J.; Leigh, D. A.; Lubomska, M.; Mendoza, S. M.; Pérez, E. M.; Rudolf, P.; Teobaldi, G.; Zerbetto, F. Macroscopic transport by synthetic molecular machines. *Nat. Mater.* **2005**, *4*, 704–710. (b) Liu, Y.; Flood, A. H.; Bonvallet, P. A.; Vignon, S. A.; Northrop, B. H.; Tseng, H.-R.; Jeppesen, J. O.; Huang, T. J.; Brough, B.; Baller, M.; Magonov, S.; Solares, S. D.; Goddard, W. A.; Ho, C.-

M.; Stoddart, J. F. Linear Artificial Molecular Muscles. *J. Am. Chem. Soc.* **2005**, *127*, 9745–9759. (c) Bruns, C. J.; Stoddart, J. F. Rotaxane-Based Molecular Muscles. *Acc. Chem. Res.* **2014**, *47*, 2186–2199.

(9) (a) Hsueh, S.-Y.; Kuo, C.-T.; Lu, T.-W.; Lai, C.-C.; Liu, Y.-H.; Hsu, H.-F.; Peng, S.-M.; Chen, C.-h.; Chiu, S.-H. Acid/Base- and Anion-Controllable Organogels Formed From a Urea-Based Molecular Switch. *Angew. Chem., Int. Ed.* **2010**, *49*, 9170–9173. (b) Goujon, A.; Lang, T.; Mariani, G.; Moulin, E.; Fuks, G.; Raya, J.; Buhler, E.; Giuseppone, N. Bistable [c2] Daisy Chain Rotaxanes as Reversible Muscle-like Actuators in Mechanically Active Gels. *J. Am. Chem. Soc.* **2017**, *139*, 14825–14828. (c) Arumugaperumal, R.; Raghunath, P.; Lin, M.-C.; Chung, W.-S. Distinct Nanostructures and Organogel Driven by Reversible Molecular Switching of a Tetraphenylethene-Involving Calix[4]arene-Based Amphiphilic [2]Rotaxane. *Chem. Mater.* **2018**, *30*, 7221–7233.

(10) (a) Pérez, E. M.; Dryden, D. T. F.; Leigh, D. A.; Teobaldi, G.; Zerbetto, F. A Generic Basis for Some Simple Light-Operated Mechanical Molecular Machines. *J. Am. Chem. Soc.* **2004**, *126*, 12210–12211. (b) Leigh, D. A.; Morales, M. A. F.; Pérez, E. M.; Wong, J. K. Y.; Saiz, C. G.; Slawin, A. M. Z.; Carmichael, A. J.; Haddleton, D. M.; Brouwer, A. M.; Buma, W. J.; Wurpel, G. W. H.; León, S.; Zerbetto, F. Patterning through Controlled Submolecular Motion: Rotaxane-Based Switches and Logic Gates that Function in Solution and Polymer Films. *Angew. Chem., Int. Ed.* **2005**, *44*, 3062–3067. (c) Ma, X.; Zhang, J.; Cao, J.; Yao, X.; Cao, T.; Gong, Y.; Zhao, C.; Tian, H. A room temperature phosphorescence encoding [2]rotaxane molecular shuttle. *Chem. Sci.* **2016**, *7*, 4582–4588. (d) Ghosh, A.; Paul, I.; Adlung, M.; Wickleder, C.; Schmittel, M. Oscillating Emission of [2]Rotaxane Driven by Chemical Fuel. *Org. Lett.* **2018**, *20*, 1046–1049. (e) Liu, Y.; Zhang, Q.; Jin, W.-H.; Xu, T.-Y.; Qu, D.-H.; Tian, H. Bistable [2]rotaxane encoding an orthogonally tunable fluorescent molecular system including white-light emission. *Chem. Commun.* **2018**, *54*, 10642–10645. (f) Sagara, Y.; Karman, M.; Seki, A.; Pannipara, M.; Tamaoki, N.; Weder, C. Rotaxane-Based Mechanophores Enable Polymers with Mechanically Switchable White Photoluminescence. *ACS Cent. Sci.* **2019**, *5*, 874–881. (g) Zhang, H.; Shao, X.; Chipot, C.; Cai, W. pH-Controlled Fluorescence Probes for Rotaxane Isomerization. *J. Phys. Chem. C* **2019**, *123*, 11304–11309.

(11) (a) Evans, N. H. Chiral Catenanes and Rotaxanes: Fundamentals and Emerging Applications. *Chem. - Eur. J.* **2018**, *24*, 3101–3112. (b) Jamieson, E. M. G.; Modicom, F.; Goldup, S. M. Chirality in rotaxanes and catenanes. *Chem. Soc. Rev.* **2018**, *47*, 5266–5311.

(12) In general, we followed the terminology adopted by Goldup and co-workers to study chirality in interlocked architectures. See ref 11b.

(13) (a) Bordoli, R. J.; Goldup, S. M. An Efficient Approach to Mechanically Planar Chiral Rotaxanes. *J. Am. Chem. Soc.* **2014**, *136*, 4817–4820. (b) Jinks, M. A.; de Juan, A.; Denis, M.; Fletcher, C. J.; Galli, M.; Jamieson, E. M. G.; Modicom, F.; Zhang, Z.; Goldup, S. M. Stereoselective Synthesis of Mechanically Planar Chiral Rotaxanes. *Angew. Chem., Int. Ed.* **2018**, *57*, 14806–14810. (c) Corra, S.; de Vet, C.; Groppi, J.; La Rosa, M.; Silvi, S.; Baroncini, M.; Credi, A. Chemical On/Off Switching of Mechanically Planar Chirality and Chiral Anion Recognition in a [2]Rotaxane Molecular Shuttle. *J. Am. Chem. Soc.* **2019**, *141*, 9129–9133. (d) Gell, C. E.; McArdle-Ismagulov, T. A.; Evans, N. H. Modulating the expression of chirality in a mechanically chiral rotaxane. *Chem. Commun.* **2019**, *55*, 1576–1579.

(14) (a) Alvarez-Pérez, M.; Goldup, S. M.; Leigh, D. A.; Slawin, A. M. Z. A Chemically-Driven Molecular Information Ratchet. *J. Am. Chem. Soc.* **2008**, *130*, 1836–1838. (b) Carlone, A.; Goldup, S. M.; Lebrasseur, N.; Leigh, D. A.; Wilson, A. A Three-Compartment Chemically-Driven Molecular Information Ratchet. *J. Am. Chem. Soc.* **2012**, *134*, 8321–8323. (c) Matsuoka, Y.; Mutoh, Y.; Azumaya, I.; Kikkawa, S.; Kasama, T.; Saito, S. Synthesis and Shuttling Behavior of [2]Rotaxanes with a Pyrrole Moiety. *J. Org. Chem.* **2016**, *81*, 3479–3487.

(15) (a) Tachibana, Y.; Kihara, N.; Takata, T. Asymmetric Benzoin Condensation Catalyzed by Chiral Rotaxanes Tethering a Thiazolium Salt Moiety via the Cooperation of the Component: Can Rotaxane Be an Effective Reaction Field? *J. Am. Chem. Soc.* **2004**, *126*, 3438–3439.

(b) Blanco, V.; Leigh, D. A.; Marcos, V.; Morales-Serna, J. A.; Nussbaumer, A. L. A Switchable [2]Rotaxane Asymmetric Organocatalyst That Utilizes an Acyclic Chiral Secondary Amine. *J. Am. Chem. Soc.* **2014**, *136*, 4905–4908. (c) Hoekman, S.; Kitching, M. O.; Leigh, D. A.; Pappmeyer, M.; Roke, D. Goldberg Active Template Synthesis of a [2]Rotaxane Ligand for Asymmetric Transition-Metal Catalysis. *J. Am. Chem. Soc.* **2015**, *137*, 7656–7659. (d) Cakmak, Y.; Erbas-Cakmak, S.; Leigh, D. A. Asymmetric Catalysis with a Mechanically Point-Chiral Rotaxane. *J. Am. Chem. Soc.* **2016**, *138*, 1749–1751. (e) Xu, K.; Nakazono, K.; Takata, T. Design of Rotaxane Catalyst for O-Acylation Asymmetric Desymmetrization of *meso*-1,2-Diol Utilizing the Cooperative Effect of the Components. *Chem. Lett.* **2016**, *45*, 1274–1276. (f) Martínez-Cuevas, A.; Marin-Luna, M.; Alonso, D. A.; Ros-Ñíguez, D.; Alajarin, M.; Berna, J. Interlocking the Catalyst: Thread versus Rotaxane-Mediated Enantiodivergent Michael Addition of Ketones to  $\beta$ -Nitrostyrene. *Org. Lett.* **2019**, *21*, 5192–5196.

(16) (a) Mitra, R.; Thiele, M.; Octa-Smolín, F.; Letzel, M. C.; Niemeyer, J. A bifunctional chiral [2]catenane based on 1,1'-binaphthyl-phosphates. *Chem. Commun.* **2016**, *52*, 5977–5980. (b) Lim, J. Y. C.; Marques, I.; Félix, V.; Beer, P. D. Enantioselective Anion Recognition by Chiral Halogen-Bonding [2]Rotaxanes. *J. Am. Chem. Soc.* **2017**, *139*, 12228–12239. (c) Lim, J. Y. C.; Marques, I.; Félix, V.; Beer, P. D. A Chiral Halogen-Bonding [3]Rotaxane for the Recognition and Sensing of Biologically Relevant Dicarboxylate Anions. *Angew. Chem., Int. Ed.* **2018**, *57*, 584–588.

(17) Berova, N.; Polavarapu, P. L.; Nakanishi, K.; Woody, R. W., Eds. *Comprehensive Chiroptical Spectroscopy*; John Wiley & Sons: New York, 2012; Vol. 1.

(18) Riehl, J. P.; Richardson, F. S. Circularly polarized luminescence spectroscopy. *Chem. Rev.* **1986**, *86*, 1–16.

(19) (a) Kumar, J.; Nakashima, T.; Kawai, T. Circularly Polarized Luminescence in Chiral Molecules and Supramolecular Assemblies. *J. Phys. Chem. Lett.* **2015**, *6*, 3445–3452. (b) Sánchez-Carnerero, E. M.; Agarrabeitia, A. R.; Moreno, F.; Maroto, B. L.; Müller, G.; Ortiz, M. J.; de la Moya, S. Circularly Polarized Luminescence from Simple Organic Molecules. *Chem. - Eur. J.* **2015**, *21*, 13488–13500. (c) Zinna, F.; Di Bari, L. Lanthanide Circularly Polarized Luminescence: Bases and Applications. *Chirality* **2015**, *27*, 1–13. (d) Longhi, G.; Castiglioni, E.; Koshoubu, J.; Mazzeo, G.; Abbate, S. Circularly Polarized Luminescence: A Review of Experimental and Theoretical Aspects. *Chirality* **2016**, *28*, 696–707.

(20) (a) Morcillo, S. P.; Miguel, D.; Álvarez de Cienfuegos, L.; Justicia, J.; Abbate, S.; Castiglioni, E.; Bour, C.; Ribagorda, M.; Cárdenas, D. J.; Paredes, J. M.; Crovetto, L.; Choquesillo-Lazarte, D.; Mota, A. J.; Carreño, M. C.; Longhi, G.; Cuerva, J. M. Stapled helical *o*-OPE foldamers as new circularly polarized luminescence emitters based on carbophilic interactions with Ag(I)-sensitivity. *Chem. Sci.* **2016**, *7*, 5663–5670. (b) Hellou, N.; Srebro-Hooper, M.; Favereau, L.; Zinna, F.; Caytan, E.; Toupet, L.; Dorcet, V.; Jean, M.; Vanthuyne, N.; Williams, J. A. G.; Di Bari, L.; Autschbach, J.; Crassous, J. Enantiopure Cycloiridiated Complexes Bearing a Pentahelicenic N-Heterocyclic Carbene and Displaying Long-Lived Circularly Polarized Phosphorescence. *Angew. Chem., Int. Ed.* **2017**, *56*, 8236–8239. (c) Sato, S.; Yoshii, A.; Takahashi, S.; Furumi, S.; Takeuchi, M.; Isobe, H. Chiral intertwined spirals and magnetic transition dipole moments dictated by cylinder helicity. *Proc. Natl. Acad. Sci. U. S. A.* **2017**, *114*, 13097–13101. (d) Schulte, T. R.; Holstein, J. J.; Krause, L.; Michel, R.; Stalke, D.; Sakuda, E.; Umakoshi, K.; Longhi, G.; Abbate, S.; Clever, G. H. Chiral-at-Metal Phosphorescent Square-Planar Pt(II)-Complexes from an Achiral Organometallic Ligand. *J. Am. Chem. Soc.* **2017**, *139*, 6863–6866. (e) Cruz, C. M.; Castro-Fernández, S.; Maçôas, E.; Cuerva, J. M.; Campaña, A. G. Undecabenz[7]-superhelicene: A Helical Nanographene Ribbon as a Circularly Polarized Luminescence Emitter. *Angew. Chem., Int. Ed.* **2018**, *57*,

- 14782–14786. (f) Cruz, C. M.; Márquez, I. R.; Mariz, I. F. A.; Blanco, V.; Sánchez-Sánchez, C.; Sobrado, J. M.; Martín-Gago, J. A.; Cuerva, J. M.; Maçôas, E.; Campaña, A. G. Enantiopure distorted ribbon-shaped nanographene combining two-photon absorption-based upconversion and circularly polarized luminescence. *Chem. Sci.* **2018**, *9*, 3917–3924. (g) Reiné, P.; Justicia, J.; Morcillo, S. P.; Abbate, S.; Vaz, B.; Ribagorda, M.; Orte, Á.; Álvarez de Cienfuegos, L.; Longhi, G.; Campaña, A. G.; Miguel, D.; Cuerva, J. M. Pyrene-Containing *ortho*-Oligo(phenylene)ethynylene Foldamer as a Ratiometric Probe Based on Circularly Polarized Luminescence. *J. Org. Chem.* **2018**, *83*, 4455–4463. (h) Zinna, F.; Voci, S.; Arrico, L.; Brun, E.; Homberg, A.; Bouffier, L.; Funaioli, T.; Lacour, J.; Sojic, N.; Di Bari, L. Circularly-Polarized Electrochemiluminescence from a Chiral Bispirene Organic Macrocycle. *Angew. Chem., Int. Ed.* **2019**, *58*, 6952–6956.
- (21) (a) Di Nuzzo, D.; Kulkarni, C.; Zhao, B.; Smolinsky, E.; Tassinari, F.; Meskers, S. C. J.; Naaman, R.; Meijer, E. W.; Friend, R. H. High Circular Polarization of Electroluminescence Achieved via Self-Assembly of a Light-Emitting Chiral Conjugated Polymer into Multidomain Cholesteric Films. *ACS Nano* **2017**, *11*, 12713–12722. (b) Imai, Y.; Nakano, Y.; Kawai, T.; Yuasa, J. A Smart Sensing Method for Object Identification Using Circularly Polarized Luminescence from Coordination-Driven Self-Assembly. *Angew. Chem., Int. Ed.* **2018**, *57*, 8973–8978. (c) Zheng, H.; Li, W.; Li, W.; Wang, X.; Tang, Z.; Zhang, S. X.-A.; Xu, Y. Uncovering the Circular Polarization Potential of Chiral Photonic Cellulose Films for Photonic Applications. *Adv. Mater.* **2018**, *30*, 1705948. (d) Chen, W.; Zhang, S.; Zhou, M.; Zhao, T.; Qin, X.; Liu, X.; Liu, M.; Duan, P. Two-Photon Absorption-Based Upconverted Circularly Polarized Luminescence Generated in Chiral Perovskite Nanocrystals. *J. Phys. Chem. Lett.* **2019**, *10*, 3290–3295. (e) Jin, X.; Sang, Y.; Shi, Y.; Li, Y.; Zhu, X.; Duan, P.; Liu, M. Optically Active Upconverting Nanoparticles with Induced Circularly Polarized Luminescence and Enantioselectively Triggered Photopolymerization. *ACS Nano* **2019**, *13*, 2804–2811.
- (22) (a) Maeda, H.; Bando, Y.; Shimomura, K.; Yamada, I.; Naito, M.; Nobusawa, K.; Tsumatori, H.; Kawai, T. Chemical-Stimuli-Controllable Circularly Polarized Luminescence from Anion-Responsive  $\pi$ -Conjugated Molecules. *J. Am. Chem. Soc.* **2011**, *133*, 9266–9269. (b) Hashimoto, Y.; Nakashima, T.; Shimizu, D.; Kawai, T. Photoswitching of an intramolecular chiral stack in a helical tetrathiazole. *Chem. Commun.* **2016**, *52*, 5171–5174. (c) Isla, H.; Srebro-Hooper, M.; Jean, M.; Vanthuyne, N.; Roisnel, T.; Lunkley, J. L.; Muller, G.; Williams, J. A. G.; Autschbach, J.; Crassous, J. Conformational changes and chiroptical switching of enantiopure bis-helicenic terpyridine upon Zn<sup>2+</sup> binding. *Chem. Commun.* **2016**, *52*, 5932–5935. (d) Homberg, A.; Brun, E.; Zinna, F.; Pascal, S.; Górecki, M.; Monnier, L.; Besnard, C.; Pescitelli, G.; Di Bari, L.; Lacour, J. Combined reversible switching of ECD and quenching of CPL with chiral fluorescent macrocycles. *Chem. Sci.* **2018**, *9*, 7043–7052. (e) Reiné, P.; Ortuño, A. M.; Resa, S.; Álvarez de Cienfuegos, L.; Blanco, V.; Ruedas-Rama, M. J.; Mazzeo, G.; Abbate, S.; Lucotti, A.; Tommasini, M.; Guisán-Ceinos, S.; Ribagorda, M.; Campaña, A. G.; Mota, A.; Longhi, G.; Miguel, D.; Cuerva, J. M. OFF/ON switching of circularly polarized luminescence by oxophilic interaction of homochiral sulfoxide-containing *o*-OPEs with metal cations. *Chem. Commun.* **2018**, *54*, 13985–13988. (f) Takaishi, K.; Yasui, M.; Ema, T. Binaphthyl-Bipyridyl Cyclic Dyads as a Chiroptical Switch. *J. Am. Chem. Soc.* **2018**, *140*, 5334–5338. (g) Imai, Y.; Yuasa, J. Off–off–on chiroptical property switching of a pyrene luminophore by stepwise helicate formation. *Chem. Commun.* **2019**, *55*, 4095–4098.
- (23) (a) Asakawa, M.; Brancato, G.; Fanti, M.; Leigh, D. A.; Shimizu, T.; Slawin, A. M. Z.; Wong, J. K. Y.; Zerbetto, F.; Zhang, S. Switching “On” and “Off” the Expression of Chirality in Peptide Rotaxanes. *J. Am. Chem. Soc.* **2002**, *124*, 2939–2950. (b) Bottari, G.; Leigh, D. A.; Pérez, E. M. Chiroptical Switching in a Bistable Molecular Shuttle. *J. Am. Chem. Soc.* **2003**, *125*, 13360–13361.
- (24) (a) Inouye, M.; Hayashi, K.; Yonenaga, Y.; Itou, T.; Fujimoto, K.; Uchida, T.-a.; Iwamura, M.; Nozaki, K. A Doubly Alkynylpyrene-Threaded [4]Rotaxane That Exhibits Strong Circularly Polarized Luminescence from the Spatially Restricted Excimer. *Angew. Chem., Int. Ed.* **2014**, *53*, 14392–14396. (b) Hayashi, K.; Miyaoka, Y.; Ohishi, Y.; Uchida, T.-a.; Iwamura, M.; Nozaki, K.; Inouye, M. Observation of Circularly Polarized Luminescence of the Excimer from Two Perylene Cores in the Form of [4]Rotaxane. *Chem. - Eur. J.* **2018**, *24*, 14613–14616.
- (25) The prefix (*R*) or (*S*) refers to the configuration of the chiral stereogenic center within the phenylalanine residue.
- (26) Saito, S.; Hirano, Y.; Mutoh, Y.; Kasama, T. Synthesis of a Homochiral [2]Rotaxane from a BINOL-derived Macrocyclic Phenanthroline. *Chem. Lett.* **2015**, *44*, 1509–1511.
- (27) (a) Ishiwari, F.; Fukasawa, K.-i.; Sato, T.; Nakazono, K.; Koyama, Y.; Takata, T. A Rational Design for the Directed Helicity Change of Polyacetylene Using Dynamic Rotaxane Mobility by Means of Through-Space Chirality Transfer. *Chem. - Eur. J.* **2011**, *17*, 12067–12075. (b) Suzuki, S.; Ishiwari, F.; Nakazono, K.; Takata, T. Reversible helix–random coil transition of poly(*m*-phenylenediethynylene) by a rotaxane switch. *Chem. Commun.* **2012**, *48*, 6478–6480.
- (28) Kuwahara, S.; Chamura, R.; Tsuchiya, S.; Ikeda, M.; Habata, Y. Chirality transcription and amplification by [2]pseudorotaxanes. *Chem. Commun.* **2013**, *49*, 2186–2188.
- (29) (a) Coutrot, F.; Busseron, E. A New Glycorotaxane Molecular Machine Based on an Anilinium and a Triazolium Station. *Chem. - Eur. J.* **2008**, *14*, 4784–4787. (b) Chao, S.; Romuald, C.; Fournel-Marotte, K.; Clavel, C.; Coutrot, F. A Strategy Utilizing a Recyclable Macrocyclic Transporter for the Efficient Synthesis of a Triazolium-Based [2]Rotaxane. *Angew. Chem., Int. Ed.* **2014**, *53*, 6914–6919. (c) Coutrot, F. A Focus on Triazolium as a Multipurpose Molecular Station for pH-Sensitive Interlocked Crown-Ether-Based Molecular Machines. *ChemistryOpen* **2015**, *4*, 556–576. (d) Waelès, P.; Fournel-Marotte, K.; Coutrot, F. Distinguishing Two Ammonium and Triazolium Sites of Interaction in a Three-Station [2]Rotaxane Molecular Shuttle. *Chem. - Eur. J.* **2017**, *23*, 11529–11539.
- (30) (a) Meng, Z.; Xiang, J.-F.; Chen, C.-F. Directional Molecular Transportation Based on a Catalytic Stopper-Leaving Rotaxane System. *J. Am. Chem. Soc.* **2016**, *138*, 5652–5658. (b) Erbas-Cakmak, S.; Fielden, S. D. P.; Karaca, U.; Leigh, D. A.; McTernan, C. T.; Tetlow, D. J.; Wilson, M. R. Rotary and linear molecular motors driven by pulses of a chemical fuel. *Science* **2017**, *358*, 340–343.
- (31) Mislow, K.; Siegel, J. Stereoisomerism and local chirality. *J. Am. Chem. Soc.* **1984**, *106*, 3319–3328.
- (32) Koreeda, M.; Gopalaswamy, R. Regio- and Stereocontrolled Synthesis of the Bay-Region anti-Diol Epoxide Metabolites of the Potent Carcinogens Benzo[a]pyrene and 7,12-Dimethylbenz[a]anthracene. *J. Am. Chem. Soc.* **1995**, *117*, 10595–10596.
- (33) (a) Giannerini, M.; Fañanás-Mastral, M.; Feringa, B. L. Direct catalytic cross-coupling of organolithium compounds. *Nat. Chem.* **2013**, *5*, 667. (b) Buter, J.; Heijnen, D.; Vila, C.; Hornillos, V.; Otten, E.; Giannerini, M.; Minnaard, A. J.; Feringa, B. L. Palladium-Catalyzed, *tert*-Butyllithium-Mediated Dimerization of Aryl Halides and Its Application in the Atroposelective Total Synthesis of Mastigophorene A. *Angew. Chem., Int. Ed.* **2016**, *55*, 3620–3624.
- (34) (a) Rostovtsev, V. V.; Green, L. G.; Fokin, V. V.; Sharpless, K. B. A Stepwise Huisgen Cycloaddition Process: Copper(I)-Catalyzed Regioselective “Ligation” of Azides and Terminal Alkynes. *Angew. Chem., Int. Ed.* **2002**, *41*, 2596–2599. (b) Tornøe, C. W.; Christensen, C.; Meldal, M. Peptidotriazoles on Solid Phase: [1,2,3]-Triazoles by Regiospecific Copper(I)-Catalyzed 1,3-Dipolar Cycloadditions of Terminal Alkynes to Azides. *J. Org. Chem.* **2002**, *67*, 3057–3064. (c) Hänni, K. D.; Leigh, D. A. The application of CuAAC ‘click’ chemistry to catenane and rotaxane synthesis. *Chem. Soc. Rev.* **2010**, *39*, 1240–1251.
- (35) A similar effect has been previously observed, although to a lesser extent, in a related pseudorotaxane; see ref 28.
- (36) Similar chemical shift ( $\delta = 2.5$  ppm) and shifting ( $\Delta\delta = -0.67$  ppm) were observed upon rotaxane formation in a related system based on a thread featuring the same phenylalanine-derived ammonium motif. See ref 15b.

(37) For some examples of CPL studies of binaphthyl derivatives, see: (a) Amako, T.; Kimoto, T.; Tajima, N.; Fujiki, M.; Imai, Y. A comparison of circularly polarized luminescence (CPL) and circular dichroism (CD) characteristics of four axially chiral binaphthyl-2,2'-diyl hydrogen phosphate derivatives. *Tetrahedron* **2013**, *69*, 2753–2757. (b) Sato, T.; Tajima, N.; Ueno, H.; Harada, T.; Fujiki, M.; Imai, Y. Binaphthyl luminophores with triphenylsilyl groups: sign inversion of circularly polarized luminescence and circular dichroism. *Tetrahedron* **2016**, *72*, 7032–7038. (c) Kitatobe, T.; Mimura, Y.; Tsujimoto, S.; Tajima, N.; Fujiki, M.; Imai, Y. Circularly polarized luminescence from open- and closed-style axially chiral amphipathic binaphthyl fluorophores in water. *Tetrahedron* **2017**, *73*, 6856–6862.

(38) Tanaka, H.; Inoue, Y.; Mori, T. Circularly Polarized Luminescence and Circular Dichroisms in Small Organic Molecules: Correlation between Excitation and Emission Dissymmetry Factors. *ChemPhotoChem*. **2018**, *2*, 386–402.

(39) For a recent example of a hemiindigo switch, which can undergo a photochemically induced switching of the ECD while the absorption intensity remains high, see: Petermayer, C.; Dube, H. Circular Dichroism Photoswitching with a Twist: Axially Chiral Hemiindigo. *J. Am. Chem. Soc.* **2018**, *140*, 13558–13561.

(40) To ensure that the “on” and “off” states of the systems show responses that are significantly different, a statistical test was performed on the signals obtained for (S)-1-H<sup>+</sup>·2PF<sub>6</sub><sup>-</sup>, (S)-1·PF<sub>6</sub><sup>-</sup>, and (S)-1·PF<sub>6</sub><sup>-</sup> after reprotonation and the data for the cycles in Figure 7. See section 7 in the [Supporting Information](#).

(41) During the peer reviewing, it was pointed out by the reviewers that another possible interference with the switching might come from the increasing amount of salts in the media after each cycle. This fact increases the ionic strength of the solution, which could disrupt the hydrogen-bonding interactions between the macrocycle and the ammonium unit. This effect could be magnified with the presence of K<sup>+</sup> ions that could also interact with the macrocycle.